JOURNAL OF STRUCTURAL BIOLOGY **121,** 30–40 (1998)
ARTICLE NO. SB973938

Structural Changes of the *Escherichia coli* GroEL–GroES Chaperonins upon Complex Formation in Solution: A Neutron Small Angle Scattering Study

Renata Stegmann, Elena Manakova, Manfred Röβle, and Hermann Heumann

Max-Planck-Institut für Biochemie, Am Klopferspitz 18a, D-82152 Martinsried, Germany

Sabine E. Nieba-Axmann and Andreas Plückthun

Biochemisches Institut der Universität Zürich, Winterthurerstrasse 190, CH-8057 Zürich, Switzerland

Thomas Hermann

Institut de Biologie Moléculaire et Cellulaire, UPR No. 9002 du CNRS, 15, rue René Descartes, F-67084 Strasbourg, France

Roland P. May

Institut Laue-Langevin, BP 156, F-38042 Grenoble Cedex 9, France

and

Albrecht Wiedenmann

Hahn-Meitner-Institut, Glienicker Strasse 100, D-14109 Berlin, Germany

Recieved September 9, 1997, and in revised form October 13,1997

We applied neutron scattering in conjunction with deuterium (D-) labeling in order to obtain information about the domain structure of GroEL and GroES isolated and in the complex. Each subunit of the heptameric GroES consists of two domains, a core domain (Met1 to Lys15 and Lys34 to Ala97) and an intervening loop region (Glu16 to Ala33). Neutron scattering shows that both regions change their conformation upon GroEL/GroES complex formation. The interdomain angle between the core regions of the heptameric GroES increases from 120 to 140°, leading to a less dome-like shape of GroES, and the loop regions turn inwards by 75°. The 23 C-terminal amino acids of the 14 GroEL subunits (Lys526 to Met548), which are unresolved in the crystal structure, are located either at the bottom of the cavity formed by the seven-membered GroEL ring or at the inner wall of the cavity. Upon complex formation the apical domains of GroEL move outwards, which facilitates binding of GroES at a GroEL–GroES center-to-center distance of (87 ± 8) Å. These structural changes may be important for the dissociation of the unfolded protein bound to the central cavity upon GroES binding. The overall structure determined by neutron scattering in solution tallies with the crystallographic model published after completion of this study. Differences in the conformation of GroES observed in the complex by the two methods support the view that the chaperonin complex is a flexible molecule which might switch in solution between different conformations.

Key Words: **chaperones; GroEL; GroES; neutron scattering; small angle scattering.**

INTRODUCTION

Molecular chaperones are involved in cellular protein folding in all forms of life (Ellis and Hartl, 1996; Hartl, 1996; Buchner, 1996; Lorimer, 1996). In bacteria, chloroplasts, and mitochondria the chaperonins of the Hsp60/Hsp10 class cooperate with the Hsp70 class in protein folding, assembly, and transport. The chaperonins GroEL and GroES are the *E. coli* members of the Hsp60/Hsp10 class. GroEL consists of 14 subunits of 60 kDa each, arranged in two heptameric rings with a large central cavity (Langer *et al.*, 1992). X-ray structure analysis has revealed that each

1047-8477/98 $25.00

subunit consists of three domains, an equatorial domain with a nucleotide binding site, an intermediate domain, and an apical domain (Braig *et al.*, 1994). The central cavity, the presumed binding site for the substrate protein, is lined with hydrophobic amino acids. The 23 C-terminal amino acids of each GroEL subunit, rich in methionine, display no electron density in the crystal, and appear not to be required for viability of *Escherichia coli*, even though this sequence is remarkably conserved and may be involved in heptamer assembly (McLennan *et al.*, 1993, 1994; Burnett *et al.*, 1994).

GroES is a dome-shaped heptamer of 10-kDa subunits which can stably bind to one side of the GroEL double ring. Transient binding to both sides has been discussed (Todd *et al.*, 1994; Corrales and Fersht, 1996; Sparrer *et al.*, 1997). GroES contains a mobile loop (Lys16 to Ala33) presumably involved in the interaction with GroEL (Landry *et al.*, 1993, 1996).

The structure of isolated GroEL was studied previously by several techniques, namely electron microscopy (Langer *et al.*, 1992; Chen *et al.*, 1994; Harris *et al.*, 1994; Roseman *et al.*, 1996), small angle neutron scattering (Thiyagarajan *et al.*, 1996; Stegmann *et al.*, 1997; Röβle, 1997), X-ray scattering (Igarashi *et al.*, 1995), and X-ray crystallography (Braig *et al.*, 1994, 1995). There is also a crystal structure model available for isolated GroES (Hunt *et al.*, 1996). The complex of both chaperonin components was analyzed by electron microscopy (Langer *et al.*, 1992; Chen *et al.*, 1994; Harris *et al.*, 1994; Roseman *et al.*, 1996) and very recently by X-ray crystal structure analysis (Xu *et al.*, 1997). Here we analyze the chaperonin complex in solution using small angle neutron scattering (SANS). Although SANS is a low resolution structural method, a verification, whether the crystallographic model tallies with the solution structure, is possible.

SANS permits the separate observation of GroEL and GroES in the complex. This is achieved by deuteration of one component and contrast matching of the other, unlabeled one, i.e., the unlabeled component is rendered "invisible" for neutrons by using a suitable D_2O/H_2O mixture, thus making possible, in contrast to electron microscopy, a clear identification of those parts belonging to GroEL and GroES.

For calculating a theoretical scattering curve the high resolution crystal structural information only of the isolated components has been used, since the atomic coordinates of the complex are not yet available. We used the Fourier transforms of the scattering intensity curves, the so-called distance distribution functions (Glatter, 1977), for a comparison of calculated and measured scattering information. Differences between the two data sets permitted localization of those protein domains in GroEL and GroES, which were not fully resolved by X-ray crystallography, and also permitted detection of conformational changes of the components upon complex formation. In interpreting the observed differences, the conformational space accessible to these domains was explored using molecular modeling techniques and by systematically varying their spatial arrangement. Those conformations were selected whose distance distribution function yielded the best agreement with the experimentally determined distance distribution function.

MATERIALS AND METHODS

GroEL/GroES Preparation

GroEL and GroES were isolated from *E. coli* W3110 harboring the plasmid pOF39. GroEL was purified as described previously (Landry *et al.*, 1996; Zahn *et al.*, 1994) except for an additional Q-Sepharose chromatography step in buffer A (50 mM Tris–HCl, pH 7.2, 0.1 mM EDTA, 1 mM DTT) with a 0– 500 mM NaCl gradient. The main steps in GroES purification were DEAE-Sepharose and Q-Sepharose in buffer A and S-Sepharose in 50 mM sodium succinate, pH 4.6, with a 0–500 mM NaCl gradient, followed by a purification step on Matrex Green A (Amicon) and a gel filtration. Deuterium labeled GroEL and GroES were prepared from the same *E. coli* strain grown in M63 medium (Miller, 1972) prepared in 95% D_2O and enriched with 1 mM $MgCl_2$, 0.4% (w/v) glucose, 10 μg/ml vitamin B1, and 100 μg/ml ampicillin. To adapt the cells to deuterated medium, H_2O-precultures were diluted first to 80% D_2O and then to 95% D_2O. Purification was performed in H_2O as described above. Protein concentrations were determined using the bicinchoninic acid assay (Pierce) and are always given for the oligomeric form.

Sample Preparation for SANS

Protein concentrations were estimated by the Bio-Rad assay before and after measurements. Buffers for all SANS experiments contained 8 mM Tris–HCl, pH 7.9, 30 mM KCl, 2 mM ADP, and 5 mM $MgCl_2$, and different amount of D_2O. The pH of D_2O containing buffers was corrected according to Sawata *et al.* (1995). All samples were dialyzed against the desired buffer by drop dialysis using a dialysis membrane 0.025 μm (Millipor).

The molar ratio of GroEL and GroES in the complexes was determined after scanning of the band intensities of dried Coomassie-stained native gels.

Stoichiometric amounts of the GroEL–GroES complex were prepared by mixing GroEL with a slight excess of GroES. Excess of GroES was removed by centrifugation of the complex through a 100-kDa Filtron or Amicon microconcentrator.

Neutron Scattering Experiments

Small-angle neutron scattering measurements have been performed at the SANS instruments D11 (Institut Laue-Langevin, Grenoble, France) and V4 (HMI Berlin) at sample-detector distances of 4 and 1 m. The samples were equilibrated to 10°C. Data evaluation was carried out as described previously (Lederer *et al.*, 1986). The scattering curves of GroEL, GroES, and the complex were analyzed in the concentration range from 2 to 10 mg/ml. No concentration dependence of the radii of gyration (R_g) was observed for GroEL alone and for the GroEL–GroES complex. R_g of GroES showed a slight concentration dependence. At low concentrations R_g slightly decreased, probably due to partial dissociation of GroES into its subunits.

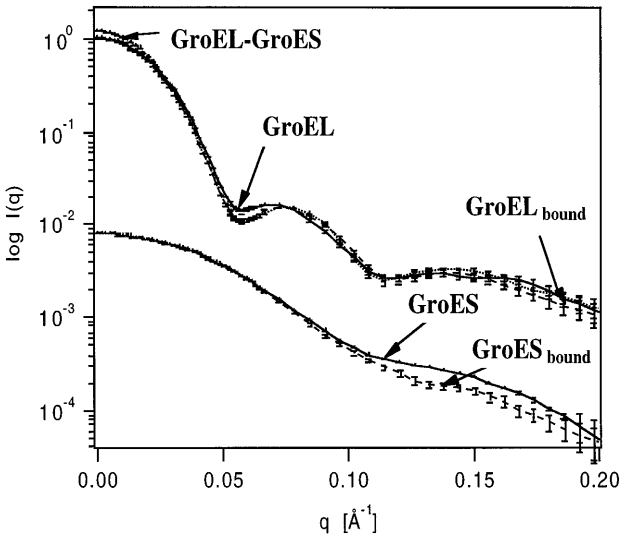

FIG. 1. The scattering curves of the chaperonin components. The scattering intensity I is shown as a function of the momentum transfer $q = 4\pi/\lambda \sin\alpha/2$ with the scattering angle α. $I(q)_{ES}$ (____) represents the scattering curve of isolated GroES, $I(q)_{ES(EL)}$ (----) of D-GroES bound in the complex, $I(q)_{EL}$ (____) of isolated GroEL, $I(q)_{EL(ES)}$ (-----) of D-GroEL bound in the complex, and $I(q)_{ES\text{-}EL}$ (·····) of the D-GroEL/D-GroES complex.

From the scattering curves the distance distribution functions $p(r)$ were calculated (Glatter, 1977), from which the maximum dimensions D_{max} of the particles were obtained. Forward scattered intensities $I(0)$ and radii of gyration R_g were determined from the area and second moment of the $p(r)$ functions, as well as from Guinier plots. From $I(0)$ the molecular weight MW_{exp} was calculated (Jacrot and Zaccai, 1981). The volume of a protein was calculated from its molecular weight assuming a partial specific volume (Durchschlag and Jaenicke, 1983) of 0.74 cm^3/g. The measurements were performed in 40% D_2O, the contrast matching D_2O concentration of unlabeled protein. Only isolated GroES was measured in 99% D_2O to achieve a better signal-to-noise ratio.

The center-to-center distance, d, of two components with radii of gyration R_1 and R_2 was determined from the radius of gyration R_g of the complex according to the parallel axes theorem of mechanics applied to scattering:

$$R^2 = z_1 R_1^2 + z_2 R_2^2 + z_1 z_2 d^2$$

z_1 and z_2 denote the scattering fraction of each component,

$$z_1 = \frac{V_i \rho_i}{V_1 \rho_1 + V_2 \rho_2}$$

with volume V_i and scattering length density ρ_i.

Alternatively, the center-to-center distance between GroEL and GroES was obtained from a Stuhrmann plot (Lederer *et al.*, 1986). Radii of gyration (R_g) were determined from a series of measurements of a GroEL/D–GroES complex at different D_2O concentrations. R_g^2 was plotted versus the inverse contrast $1/\Delta\rho$ and fitted to the parabolic equation:

$$R_g^2 = R_c^2 + \frac{\alpha}{\Delta\rho} - \frac{\beta}{\Delta\rho^2}$$

with $R_C = 59.6$ Å, the radius of gyration at infinite contrast, and the coefficients $\alpha = 3.11 \times 10^{-4}$ and $\beta = 0.720 \times 10^{-9}$ Å^{-2}. Using the coefficient β distance d is obtained according to the equation

$$d = \left(\frac{\beta}{\Delta\rho_1^2}\right)^{1/2} + \left(\frac{\beta}{\Delta\rho_2^2}\right)^{1/2}$$

$\Delta\rho_1$ and $\Delta\rho_2$ are the contrasts at which GroEL and D-GroES are matched, respectively.

Molecular Modeling

In order to explore the conformational space available to the flexible loops, we used a molecular dynamics approach. We performed simulated annealing on the loop residues Glu16 and Ala33, while the other amino acids of the GroES heptamer were constrained to their positions in the crystal. During the MD simulations in vacuum under the AMBER force field (Pearlman *et*

TABLE I

Protein	MW [kDa]	Volume [10^3 Å^3]	R_g [Å]	$I(0)$	MW_{exp} [kDa]	D_{max} [Å]
GroES isolated	70	85.4	30.7 ± 0.1	0.086 ± 0.001	83 ± 2	[94–98]
Model (crystal structure (Hunt *et al.*, 1996))			30.5			94
GroES bound to GroEL			29.9 ± 0.2	0.092 ± 0.0004		[92–96]
Model			29.7			90
GroEL isolated (our study)	798	979	62.0 ± 0.4	7.77 ± 0.04	786 ± 20	[176–182]
GroEL isolated (Igarashi *et al.*, 1995) (SAXS)			66.2			
GroEL isolated (Thiyagarajan *et al.*, 1996) (SANS)			63.2 ± 0.8			
Model (crystal structure (Braig *et al.*, 1994, 1995)			62.8			178
GroEL isolated (Langer *et al.*, 1992) (EM)						185
GroEL bound to GroES			63.5 ± 0.2	7.11 ± 0.02		[182–188]
Model			64.7			182
GroEL/GroES complex	868	1061	66.3 ± 0.2	11.1 ± 0.04	939 ± 23	[194–198]
Model			66.9			188
GroEL/GroES complex (Langer *et al.*, 1992) (EM)						215

Note. SAXS, small angle x-ray scattering; SANS, small angle neutron scattering; EM, electron microscopy. D_{max} represents the largest dimension of the molecule which is the spatial diagonal.

al., 1994), the loops were heated to 1000 K for 2000 fs, followed by slow cooling to 10 K with a linear cooling coefficient of 1 K/fs. This rather short simulation time at high temperature was sufficient to randomize the structure of the mobile loop and account for its flexibility.

The location for the GroEL C-terminal residues Lys526 to Met548, not resolved in the crystal structure analysis, was investigated by MD simulations under the AMBER force field (Pearlman *et al.*, 1994). Starting from a random conformation 100 ps of MD calculation at 300 K in vacuum were performed on the C-termini of the seven subunits within one ring while the residues Met1 to Pro525 were left unchanged with respect to the crystal structure coordinates. The distribution of the C-terminal residues within the central cavity of the GroEL heptamer was continuously monitored during the MD simulations.

Domain Modeling

In order to simulate different conformations of the GroES core domain and the mobile loop, the domains were tilted. The pivot of the core domains was the center of the upper hole formed by the tips of the GroES core domain. The core domains were tilted away from the sevenfold main axis as indicated in Fig. 2c.

For the simulation of the conformational changes of the GroES loop region upon binding to GroEL, a hinge between amino acid Glu16 and Ala33 was used as pivoting point. These two amino acids are located at the beginning and the end of the flexible loop-region. The loop was tilted in the same plane as the GroES core domain. Other orientation of the GroES core domain as well as of the mobile loop were ruled out by comparing calculated and experimentally obtained $p(r)$ (data not shown).

In order to simulate different conformations of the GroEL apical domain, a hinge between the amino acids Val190 and Ala377 was introduced. This makes sense, since the steep gradient of the temperature factors between these two amino acids indicated high flexibility of the apical domain around this region. Tilting was performed in the same plane as the GroES core domain.

RESULTS AND DISCUSSION

Solutions of isolated GroEL and GroES as well as of the GroEL–GroES complex were analyzed by SANS. Three differently D-labeled complexes were used where either of the components or both were deuterated. The resulting scattering curves (Fig. 1) permitted calculation of the radii of gyration (R_g), maximum dimensions (D_{max}), volumes, and molecular weights of the components (Jacrot and Zaccai, 1981), as shown in Table I.

The Domain Structure of Isolated GroES

Figure 2a shows the distance distribution function, $p(r)_{ES}$, of free GroES derived from the corresponding scattering curve of Fig. 1. The shoulder in $p(r)_{ES}$ at about 20 Å is characteristic for a body containing a cavity, as model calculations have revealed (data not shown). This finding is consistent with the crystal structure, which indicates that GroES has a dome-like structure (Harris *et al.*, 1994).

The experimentally obtained $p(r)_{ES}$ is well represented by $p(r)_{ESmodel}$ calculated by using the C_α-atom coordinates of the crystal structure (Hunt *et al.*, 1996) with several modifications. The peptide Glu16 to Ala33 that forms a loop region, as revealed by the GroES crystal structure (Hunt *et al.*, 1996), is crystallographically resolved in only one GroES subunit, indicating mobility of this domain. We therefore modeled the structure of the seven loops in the GroES heptamer, assuming that the conformation of the loops are all slightly different from each other to account for their disordered state in the crystal (see Materials and Methods). The resulting distance distribution function $p(r)_{ESmodel}$ agrees well with the experimentally obtained curve, indicating that there is no significant difference between the solution conformation and the crystal conformation within the resolution limits of the small angle scattering experiment.

Changes of the Domain Structure of GroES upon Complex Formation

In order to determine whether the conformation of GroES changes upon binding to GroEL, the complex was reconstituted from deuterated GroES and unlabeled GroEL. Complex formation at different molar ratios of the components was followed analytically by nondenaturing PAGE, as shown in Fig. 3. From these data a binding constant of 2×10^8 M^{-1} was estimated, assuming a 1:1 stoichiometry of GroEL and GroES.

The complex reconstituted from GroEL and D-GroES in a 1:1 stoichiometry was subjected to neutron scattering in 40% D_2O, the matching point of unlabeled GroEL (data not shown). This permitted specific observation of GroES in the complex. The scattering curve of bound GroES, $I_{ES(EL)}$, is shown in Fig. 1 and the corresponding distance distribution function, $p(r)_{ES(EL)}$, in Fig. 2b (right). This distance distribution function differs from that of the isolated $p(r)_{ES}$, indicating a conformational change of GroES

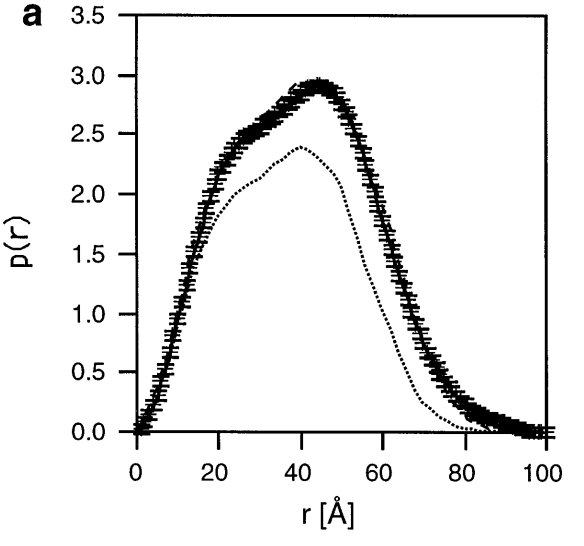

FIG. 2

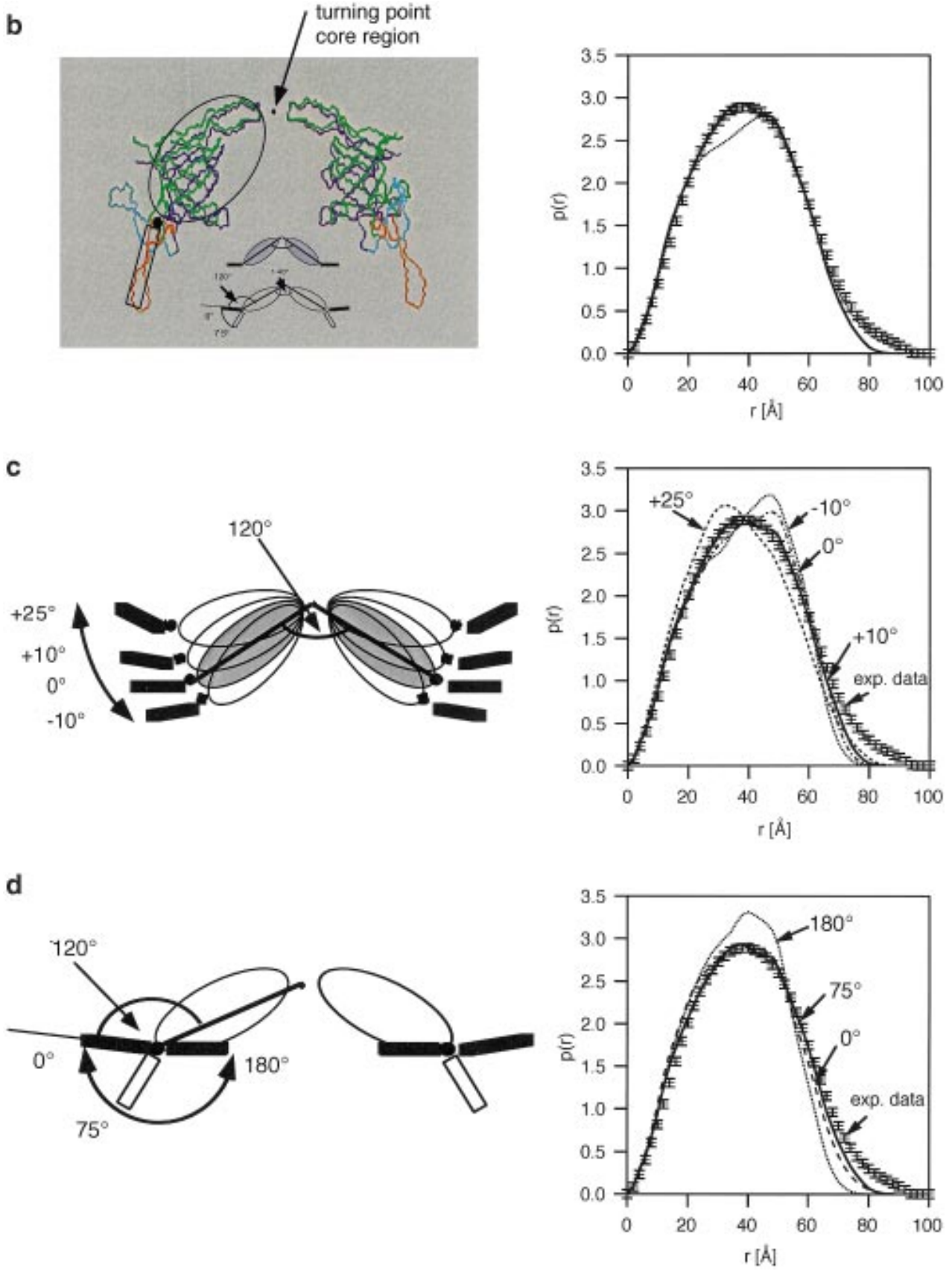

FIG. 2—*Continued*

upon complex formation. The disappearance of the shoulder in $p(r)_{ES(EL)}$ compared to $p(r)_{ES}$ indicates that the bound GroES has a less pronounced dome-like structure. Our model accounts for this change by arranging the GroES subunits in such a way that the dome-like structure of GroES becomes more open, as indicated in Fig. 2b (left) and Fig. 2c (left). The resulting distance distribution function, $p(r)_{ES(EL)model}$, representing this new arrangement, is shown in Fig. 2b (right). The distance distribution function is rather sensitive toward changes of the opening angle (Fig. 2c). Systematic variation of the angle revealed that the agreement with the experimentally determined $p(r)_{ES(EL)}$ is optimal at an opening angle of 140°, compared to 120° in the isolated GroES (Fig. 2c). Further improvement of the fit was achieved by changing the orientation of the loop region (Fig. 2d). The experimentally obtained distance distribution function was best approximated when the loop was oriented 75° inwards, with respect to the loop orientation of isolated GroES.

Thus, starting from the crystal structure of isolated GroES, we have changed two structural parameters in order to approximate the distance distribution function of GroES in the bound state, namely the opening angle of the GroES dome and the orientation of the mobile loop.

The Domain Structure of GroEL

The distance distribution function of isolated GroEL, $p(r)_{EL}$, derived from the corresponding scattering curve, I_{EL} (Fig. 1), is shown in Fig. 4a. $p(r)_{EL}$ shows a shoulder, indicating that GroEL has a cavity, consistent with electron microscopic and crystallographic studies (Langer *et al.*, 1992; Braig *et al.*, 1994; Chen *et al.*, 1994; Harris *et al.*, 1994; Braig *et al.*, 1995). Calculation of the distance distribution function from the available crystallographic data (Braig *et al.*, 1994, 1995) alone was not possible, since the amino acid region at the C-terminus, Lys526 to Met548, is unresolved. Based on a small angle scattering curve of isolated GroEL and model calculations Thiyagarajan *et al.* (1996) suggested that the unresolved part of the protein is located at the equatorial domain having a lower protein density. Our model calculations suggest two possible locations for the unresolved peptide chains. The first arrangement, represented by $p(r)_{ELmodel(a)}$ in Fig. 4a,

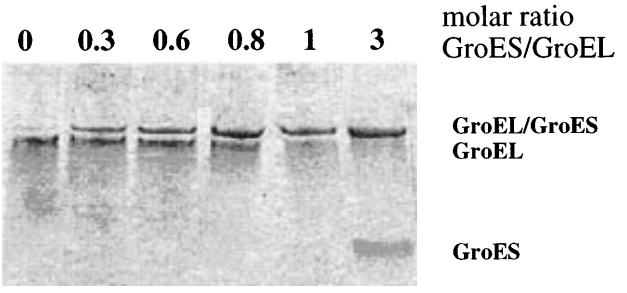

FIG. 3. Nondenaturing gel electrophoresis of the GroEL–GroES complex. GroEL (c=6.5 μM) and GroES were mixed in molar ratios as indicated using the buffer conditions described under Materials and Methods (Sample preparation for SANS). 2 μl of each sample was loaded after 10 min incubation on a 5% acrylamide gel as described by Langer *et al.* (1992). The gel contained 2 mM ADP and the running buffer 0.2 mM ADP in order to prevent dissociation of the complex.

FIG. 2. The scattering functions and the derived structures of GroES isolated and as part of the GroEL–GroES complex. (a) The distance distribution function, $p(r)_{ES}$, of isolated GroES. $p(r)_{ES}$ (____) was obtained by Fourier transform of the scattering curve, $I(q)_{ES}$, using the indirect Fourier transform program of Glatter (1977). For comparison the distance distribution function $p(r)_{E\text{-}Scrys}$ (·····) is shown which was calculated from the C_α-coordinates obtained from crystal structure analysis (Hunt *et al.*, 1996; Röβle, 1997) without the unresolved region from Glu16 to Ala33. $p(r)_{ESmodel}$ (-----) is the distance distribution function of GroES taking the unresolved parts into account as described in the text. (b) The distance distribution function, $p(r)_{ES(EL)}$, of GroES as part of the complex, and the structural model derived from the scattering functions. $p(r)_{ES(EL)}$ (____) is the experimental distance distribution function of GroES in the complex and $p(r)_{ES(EL)model}$ (-----) is the distance distribution function of the corresponding model. The model has been optimized with respect to the spatial arrangement of the core domains and the orientation of the loops. For comparison, the distance distribution function, $p(r)_{ES}$ (·····), of isolated GroES is also shown. The model on the left shows two subunits of GroES located on opposite sides. The dark blue represents the core domain in the isolated GroES subunit, whose coordinates are taken from the X-ray structure (Hunt *et al.*, 1996) and the light blue part the loop domain, whose conformation was determined as described in the text. The structure of the core domain of GroES after complex formation with GroEL is shown in green and that of the loop in red. (c) Model calculations for determining the optimal arrangement of GroES core subunits. Core subunits were systematically tilted as indicated (left side) without changing the loop structure. The corresponding distance distribution functions are shown on the right side. The shaded ellipsoid represents the spatial arrangement of the GroES core subunits in the isolated state. The optimal agreement between the experimental distance distribution function and the calculated distance distribution function was obtained, when the GroES core subunits were tilted 10° more than in the isolated GroES. The dot indicates the pivot for the core domains and the loop regions, as described under Materials and Methods. (d) Model calculations for determining the optimal orientation of the GroES loop. The angle between the core domain and the loop (Glu16 to Ala33) in isolated GroES is 120°, as indicated. This angle was systematically varied from 0 to 180° without changing the spatial arrangement of the core domain, which was kept at its optimum of a roof angle of 140°. An optimal fit of the experimentally determined $p(r)_{ES(EL)}$ was obtained at an angle of 75°, as indicated in the figure. Differences between the calculated and experimentally obtained distance distribution function at large distances around 80 Å could either be due to formation of unspecific aggregates or due to deuterated impurities (copurified with GroES) which make constructive interferences with the D-labeled GroES. Additional model calculations (data not shown) suggested the possibility that a deuterated protein having an approximate molecular weight of 10 kDa is bound to the GroEL ring opposite to GroES.

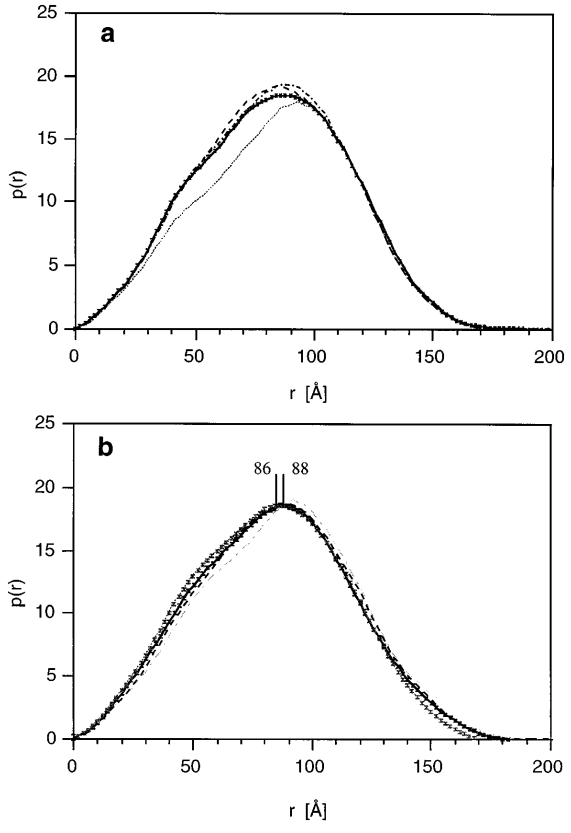

FIG. 4. The scattering functions and the derived structures of GroEL isolated and as part of the GroEL–GroES complex. (a) The distance distribution function of isolated GroEL. $p(r)_{EL}$ (____) is the experimentally determined distance distribution function, $p(r)_{ELcrys}$ (·····) is the distance distribution function calculated from the crystal coordinates, and $p(r)_{ELmodel}$ is the calculated distance distribution function including the peptides Pro526 to Met548 of the 14 GroEL subunits which are not resolved in the crystal structure. The best fit was obtained if the missing parts were located at the lower 20% of the GroEL cavity or at the wall. The distance distribution functions for the two arrangements are $p(r)_{ELmodel(a)}$ (-----) and $p(r)_{ELmodel(b)}$ (-.-.-.-), respectively. The deviation of the calculated distance distribution functions at short distances might be due to partial dissociation of GroEL into monomers, as already pointed out by Thiyagarajan *et al.* (1996). (b) The distance distribution function, $p(r)_{EL(ES)}$, of GroEL bound to GroES. $p(r)_{EL(ES)}$ (____) is the experimentally determined distance distribution function of GroEL as part of the complex. For comparison, $p(r)_{EL}$ (·····) of isolated GroEL is also shown. $p(r)_{EL(ES)(a)}$ (-----) was calculated assuming that the apical domains of all GroEL subunits within one ring turn outwards by 55°, a result which is consistent with electron microscopic studies (Chen *et al.*, 1994). Model calculations excluded the possibility that the apical domains of both GroEL rings are turned outwards by 55°, in comparison with the corresponding $p(r)_{EL(ES)(aa)}$ (-.-.-.-) indicates.

assumes that the peptide is located in the lower 20 Å of the cavities formed by the two GroEL rings, having an average density of 1.35 g/cm^3, the normal density of proteins (Durchschlag and Jaenicke, 1983). The second arrangement represented by $p(r)_{ELmodel(b)}$ is based on molecular dynamics calculations. It assumes that the unresolved peptide chains of mainly hydrophobic amino acids are located in proximity to the wall of the cavity, leaving a hole at the bottom of each GroEL ring. Whether an ADP-dependent rotation of the GroEL subunits occurs, as recently suggested by EM-studies (Roseman *et al.*, 1996), could not be judged by our studies, because scattering curves are insensitive toward rotationally symmetric changes which do not result in redistribution of masses.

Changes of the Domain Structure of GroEL upon Complex Formation

Comparison of the distance distribution function of GroEL in the complex with GroES, $p(r)_{EL(ES)}$ (Fig. 4b), with the distance distribution function of isolated GroEL shows that the $p(r)_{EL(ES)}$ peak is shifted by 2 Å to larger distances and that the maximum dimension, D_{max}, of GroEL is slightly increased in the bound state (see also Table I). This indicates that parts of the GroEL mass are displaced from the center of gravity of GroEL upon complex formation. Model calculations (compare $p(r)_{EL(ES)model(a)}$) show that the best fit is obtained if the apical domains are turned outwards by 55°. This result is consistent with electron microscopic studies (Chen *et al.*, 1994). Further model calculations (compare $p(r)_{EL(ES)model(aa)}$) also showed that the apical domains of only one GroEL ring are involved in this conformational change.

The Model of the GroEL–GroES Complex

The basis for building a model of the GroEL–GroES complex was the scattering curve, $I_{EL\text{-}ES}$ (Fig. 1), and the corresponding distance distribution function, $p(r)_{EL\text{-}ES}$ (Fig. 5b). The model was built in two steps, determining the center-to-center distance of GroEL and GroES and subsequently their orientation.

In order to determine the center-to-center distance between GroEL and GroES, the complex reconstituted from unlabeled GroEL and deuterated GroES was subjected to a contrast variation experiment; i.e., the complex was analyzed in buffer solutions having different D_2O content. By varying the D_2O content, the scattering contribution of H-GroEL and D-GroES was changed, resulting in a series of different radii of gyration (R_g). Applying the Stuhrmann approach (Ibel, 1975), a center-to-center distance of $d = (87 \pm 8)$ Å was determined from the D_2O-dependence of R_g (Fig. 5a). Approximately the same distance of $d = (85 \pm 26)$ Å was obtained if the parallel axes theorem of mechanics was applied (see Materials and Methods).

The distance distribution function of the complex (Fig. 5b and Table I) indicates that the maximum

size of the complex is 15 Å larger than GroEL alone. This suggests that GroES is located at the long axis of the GroEL cylinder, as already suggested by electron microscopic studies. We used this information and placed GroES at a distance of 87 Å from the center of gravity of GroEL. The distance distribution function of the complex, $p(r)_{\text{EL-ESmodel}}$, was calculated by using the structural information about GroEL and GroES when part of the complex. Figure 5b shows that the calculated and the experimentally obtained distance distribution functions agree within the error margins of the data. Further model calculations showed that the neutron scattering curve is insensitive toward a rotation of GroES with respect to GroEL (Röβle, 1997). Our model, in which the GroES subunits are located in-between two neighboring GroEL subunits, represents an arrangement which was obtained by placing the two components at a distance of 87 Å and rotating them along the sevenfold axis until the steric overlap is reduced to a minimum. The final model of the GroEL–GroES complex is shown in Fig. 5d (right). The crystal structure of the complex (Xu *et al.*, 1997) is shown in Fig. 5d (left) as a side projection. It is worth noting that the crystal structure of the complex has been published after the neutron scattering study has been finished. A comparison of the two models is possible even if the coordinates of the crystal structure are not yet available by direct inspection of the overall dimensions shown in Fig. 5d, along with the published information about the conformational changes in GroEL and GroES upon complex formation.

The overall structure of the two models agree within the error margins of SANS as indicated by the size parameters shown in Fig. 5d. Electron microscopic studies (Langer *et al.*, 1992; Chen *et al.*, 1994; Harris *et al.*, 1994; Roseman *et al.*, 1996) as well as the crystallographic studies (Xu *et al.*, 1997) show dramatic changes of the GroEL conformation upon complex formation, namely rotation of different GroEL domains and tilting of the apical domains. While an enlargement of GroEL due to the outward tilting of the apical domains has been observed by the neutron scattering studies, this technique is not sensitive toward domain rotation within a large molecule such as GroEL.

GroES has a shape like a jelly fish. The core domains of each of the subunits form an inner ring and the flexible domains form an outer ring. The crystallographic as well as the neutron scattering solution structure reveals that the flexible domains of GroES are tilted down upon complex formation, contacting the GroEL apical domains. The exact conformation of the flexible domain could not be determined by neutron scattering due to the limited resolution of the method. This might be the reason that the flexible domains appear to merge into GroEL more than in the crystallographic model. Despite the agreement in the global dimensions, there is a remarkable difference between the two models concerning the conformation of the GroES core domains. While the crystal structure model indicates no change of the GroES core structure upon complex formation, the neutron scattering study suggests that the conformation of the core domains is affected, namely that the roof formed by the core domains is flattened upon complex formation.

CONCLUSION

Models of GroEL and GroES in the isolated state (Fig. 5c (left)), as part of the complex (Fig. 5c (right)), and the complex as a whole (Fig. 5d (right)) were derived from neutron scattering studies performed in solution. The basis of the interpretation of the scattering curves are model calculations and crystallographic data of isolated GroEL and GroES. The domain structure of isolated GroEL and GroES determined by neutron solution studies is consistent with the crystal structure of the isolated components. This is confirmed by the agreement of different parameters and functions determined by both approaches, such as the radii of gyration, $D_{\max}$ (see Table I), and the distance distribution function. There is qualitative agreement between our models and that obtained by electron microscopic studies. A quantitative comparison of the results obtained by the two methods is difficult, since parameters, e.g., the center-to-center distance between GroEL and GroES, could only be determined by neutron scattering using deuterated components. The maximum dimension, $D_{\max}$, is a parameter which can be determined by all three methods. Table I shows that the values obtained by the various methods and for the various components differ at most by 10%, which is within the experimental error margins.

The fact that the neutron scattering curves of the isolated components could be interpreted by using the crystal coordinates shows that the crystal structure closely resembles the solution structure within the accuracy of the SANS study.

Due to this limited accuracy the dramatic changes in GroEL upon complex formation with GroES observed by the crystallographic approach could not be judged, since SANS is insensitive toward domain rotations within the large GroEL molecule.

However, the pronounced changes of the neutron scattering curve of GroES upon complex formation can only be interpreted by a conformational change of the flexible domains as well as of the central core domains. Neutron scattering indicates that upon

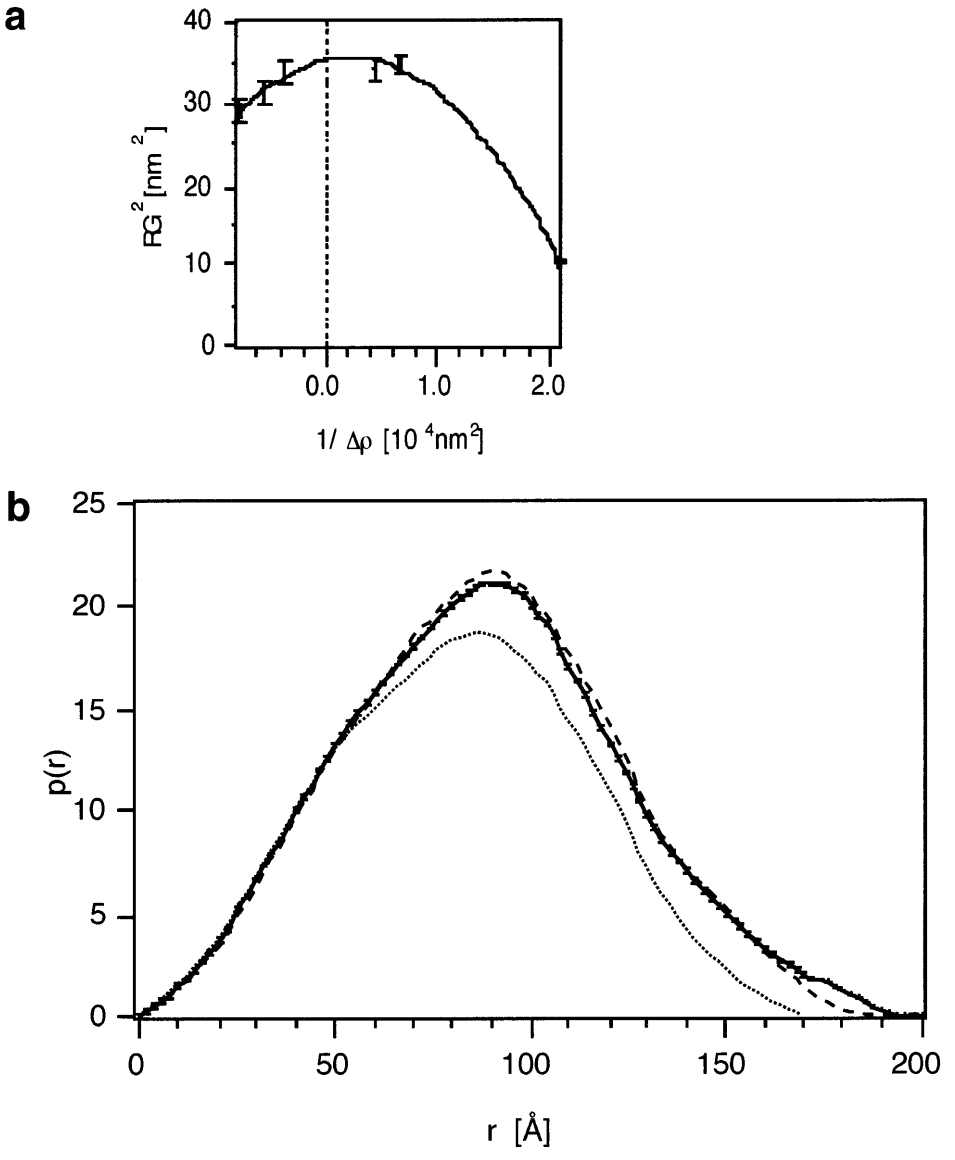

FIG. 5. The scattering functions and the derived structure of the GroEL–GroES complex. (a) Determination of the center-to-center distance of GroEL and GroES. Complex reconstituted from unlabeled GroEL and deuterated GroES was analyzed in buffers containing different D_2O concentrations. From the plot $(R_g)^2$ versus the inverse contrast $\Delta\rho$ a parabolic curve can be fitted according to the Stuhrmann equation (Ibel, 1975) (see Materials and Methods). From this equation the center-to-center distance was determined as $d = (87 \pm 8)$ Å. (b) The distance distribution function, $p(r)_{EL\text{-}ES}$, of the chaperonin complex GroEL–GroES. $p(r)_{(EL\text{-}ES)}$ (____) is the experimentally determined distance distribution function of the complex and $p(r)_{(EL\text{-}ES)model}$ (-----) is that of the model shown in d (right). For comparison, the distance distribution function $p(r)_{EL(ES)}$ (·····) of GroEL is also shown. (c) The models of the chaperonin components GroEL and GroES as determined by neutron solution scattering. The model of GroEL and GroES in the isolated state is shown on the left side; the model of both components as parts of the complex is shown on the right. GroES is displayed here three times larger with respect to GroEL. (d) Comparison of the GroEL–GroES complex as determined by X-ray crystallography and by neutron solution scattering. The model obtained by neutron scattering is shown on the right side as a projection after cutting half of the molecule. The complex was obtained by docking GroEL and GroES at a center-to-center distance of $d = 87$ Å, as described in the text. The model obtained by X-ray crystallography is a reproduction of the originally published model by Xu *et al.* (1997).

complex formation the mobile GroES loops fold down as observed with the crystal structure and the central domains of GroES become flatter with respect to the sevenfold axis, giving less of a dome shape. We suggest that the flatter GroES roof is a conformational characteristic for the solution structure of GroES in the complex and that the difference in the structure observed in the crystal and in solution is a consequence of conformational flexibility of the GroEL–GroES complex.

The SANS studies reported here provide the basis for further structural and kinetic studies of the

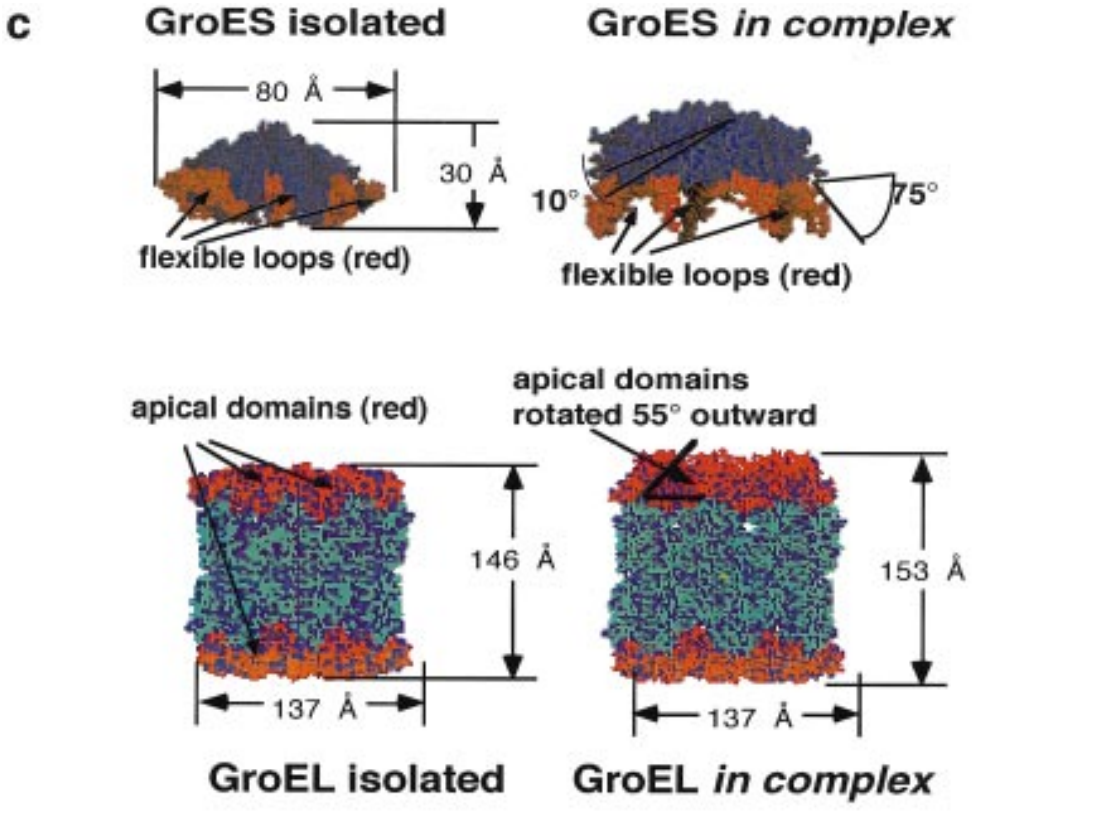
c
GroES isolated
GroES in complex
80 Å
30 Å
flexible loops (red)
10°
75°
flexible loops (red)
apical domains (red)
apical domains
rotated 55° outward
146 Å
137 Å
153 Å
137 Å
GroEL isolated
GroEL in complex

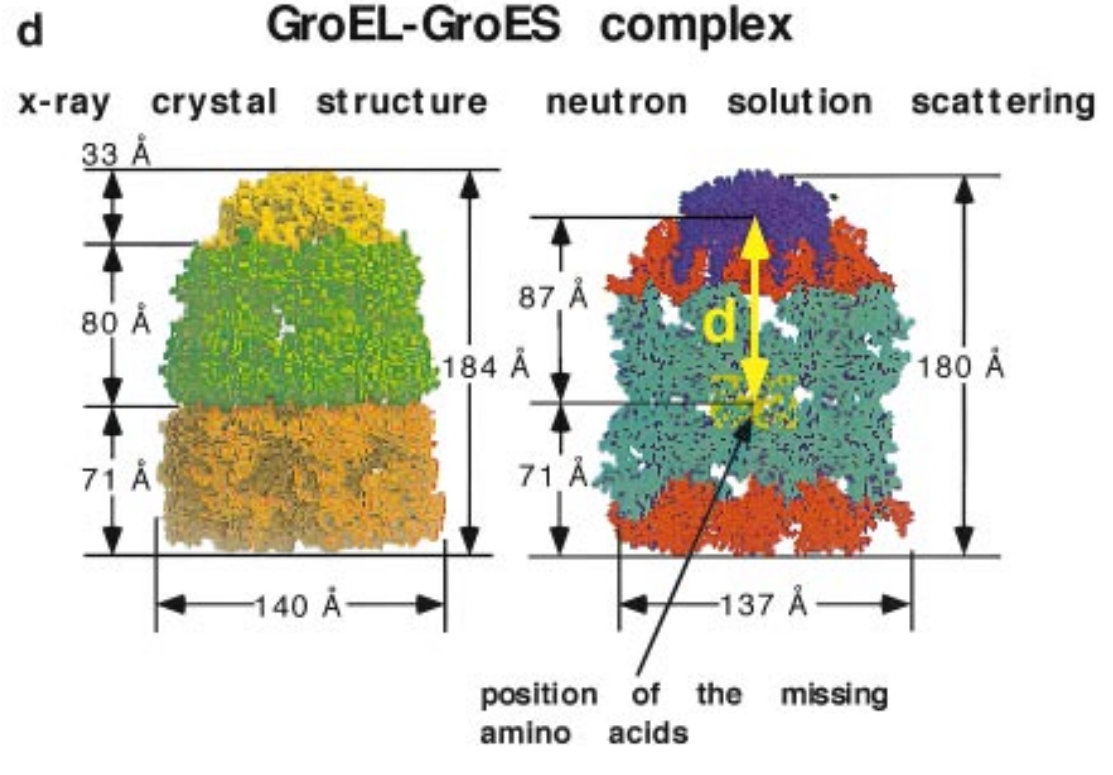
d
GroEL-GroES complex
x-ray crystal structure
neutron solution scattering
33 Å
80 Å
71 Å
184 Å
140 Å
87 Å
d
71 Å
180 Å
137 Å
position of the missing
amino acids

GroEL–GroES complex with substrate in solution, which is an important part in understanding the action of a molecular chaperone. Thus, the SANS approach complements the structural studies performed by means of X-ray analysis in the crystal and electron microscopy under nonsolution conditions.

The authors thank the DFG (He1285/13-1) and the BMBF (Grant HE4MPG) and the Swiss National Fund (Grant 3100-037720.93/1) for support.

REFERENCES

Braig, K., Adams, P. D., and Brünger, A. T. (1995) Conformational variability in the refined structure of the chaperonin GroEL at 2.8 Å resolution, *Nature Struct. Biol.* **2**, 1083–1094.

Braig, K., Otwinowski, Z., Hegde, R., Boisvert, D. C., Joachimiak, A., Horwich, A. L., and Sigler, P. B. (1994) The crystal structure of the bacterial chaperonin GroEL at 2.8 Å, *Nature* **371**, 578–586.

Buchner, J. (1996) Supervising the fold: Functional principles of molecular chaperones, *FASEB J.* **10**, 10–19.

Burnett, B. P., Horwich, A. L., and Brooks Low, K. (1994) A carboxy-terminal deletion impairs the assembly of GroEL and confers a pleiotropic phenotype in *Escherichia coli* K-12, *J. Bacteriol.* **176**, 6980–6985.

Chen, S., Roseman, A. M., Hunter, A. S., Wood, S. P., Burston, S. G., Ranson, N. A., Clarke, A. R., and Saibil, H. R. (1994) Location of a folding protein and shape changes in GroEL–GroES complexes imaged by cryo-electron microscopy, *Nature* **371**, 261–264.

Corrales, F. J., and Fersht, A. R. (1996) Kinetic significance of GroEL•GroES chaperone activity: An ATPase-gated and-pulsed folding and annealing cage, *Proc. Natl. Acad. Sci. USA* **93**, 4509–4512.

Durchschlag, H., and Jaenicke, R. (1983) Partial specific volume changes of proteins: Ultracentrifugal and viscosimetric studies, *Intl. J. Biol. Macromolecules* **5**, 143–148.

Ellis, R. J., and Hartl, F. U. (1996) Protein folding in the cell: Competing models of chaperonin function, *FASEB J.* **10**, 20–26.

Glatter, O. (1977) A new method for the evaluation of small-angle-scattering data, *J. Appl. Crystallogr.* **10**, 415–421.

Harris, J. R., Plückthun, A., and Zahn, R. (1994) Transmission electron microscopy of GroEL, GroES, and the symmetrical GroEL/ES complex, *J. Struct. Biol.* **112**, 216–230.

Hartl, F. U. (1996) Molecular chaperones in cellular protein folding, *Nature* **381**, 571–580.

Hunt, J. F., Weaver, A. J., Landry, S. J., Gierasch, L., and Deisenhofer, J. (1996) The crystal structure of the GroES co-chaperonin at 2.8 Å resolution, *Nature* **379**, 37.

Ibel, K. (1975) Comparison of neutron and X-ray scattering of dilute myoglobin solutions, *J. Mol. Biol.* **93**, 255–265.

Igarashi, Y., Kimura, K., Ichimura, K. K., Matsuzaki, S., Ikura, T., Kuwajima, K., and Kihara, H. (1995) Solution X-ray scattering study on the chaperonin GroEL from *Escherichia coli*, *Biophys. Chem.* **53**, 259–266.

Jacrot, B., and Zaccai, G. (1981) Determination of molecular weight by neutron scattering, *Biopolymers* **20**, 2413–2426.

Landry, S. J., Taher, A., Georgopoulos, C., and van der Vies, S. M. (1996) Interplay of structure and disorder in cochaperonin mobile loops, *Proc. Natl. Acad. Sci. USA* **93**, 11622–11627.

Landry, S. J., Zeilstra-Ryalls, J., Fayet, O., Georgopoulos, C., and Gierasch, L. M. (1993) Characterisation of a functionally important mobile domain of GroES, *Nature* **364**, 255–258.

Langer, T., Pfeifer, G., Martin, J., Baumeister, W., and Hartl, F. U. (1992) Chaperonin-mediated protein folding: GroES binds to one end of the GroEL cylinder, which accommodates the protein substrate within its central cavity, *EMBO J.* **11**, 4757.

Lederer, H., May, R. P., Kjems, J. K., Schaefer, W., Crespi, H. L., and Heumann, H. (1986) Deuterium incorporation into Escherichia coli proteins: A neutron-scattering study of DNA-dependent RNA polymerase, *Eur. J. Biochem.* **156**, 655–660.

Lorimer, G. H. (1996) A quantitative assessment of the role of chaperonin proteins in protein folding *in vivo*, *FASEB J.* **10**, 5–9.

McLennan, N. F., Girshovich, A. S., Lissin, N. M., Charters, Y., and Masters, M. (1993) The strongly conserved carboxyl-terminus glycine-methionine motif of the *Escherichia coli* GroEL chaperonin is dispensable, *Mol. Microbiol.* **7**, 49–58.

McLennan, N. F., McAteer, S., and Masters, M. (1994) The tail of a chaperonin: The C-terminal region of *Escherichia coli* GroEL protein, *Mol. Microbiol.* **14**, 309–321.

Miller, J. H. (1972) *in* Experiments in Molecular Genetics, p. 431, Cold Spring Harbor Laboratory, Cold Spring Harbor, New York.

Moore, P. B. (1980) Small-angle scattering. Information content and error analysis, *J. Appl. Crystallogr.* **13**, 168–175.

Pearlman, D. A., Case, D. A., Caldwell, J. W., Ross, W. S., Cheatham, T. E., DeBolt, S., Ferguson, D., Seibel, G., Singh, U. C., Weiner, P. K., and Kollman, P. A. (1994) AMBER 4.1, San Francisco, CA.

Roseman, A. M., Chen, S., White, H., Braig, K., and Saibil, H. R. (1996) The chaperonin ATPase cycle: mechanism of allosteric switching and movements of substrate-binding domains in GroEL, *Cell* **87**, 241–251.

Röβle, M. (1997) Untersuchungen zur Struktur und Funktion des *Escherichia coli* Chaperoninsystems GroEL und GroES mit Hilfe der Neutronenkleinwinkelstreuung, Diploma thesis, LMU München.

Sawata, S., Komiyama, M., and Taira K. (1995) Kinetic evidence based on solvent isotope effects for the nonexistence of a proton-transfer process in reactions catalyzed by a hammerhead ribozyme: implication to the double-metal-ion mechanism of catalysis, *J. Am. Chem. Soc.* **117**, 2357–2358.

Sparrer, H., Rutkat, K., and Buchner J. (1997) Catalysis of protein folding by symmetric chaperone complexes, *Proc. Natl. Acad. Sci. USA* **94**, 1096–1100.

Stegmann, R., Manakova, E., Axmann, S., Röβle, M., Hermann, T., May, R. P., Wiedenmann, A., Plückthun, A., and Heumann, H. (1997) Conformational changes and spatial arrangement of the *E. coli* chaperones GroEL and GroES, *Physica B* **234**, 220–222.

Thiyagarajan, P., Henderson, S. J., and Joachimiak A. (1996) Solution structures of GroEL and its complex with rhodanese from small-angle neutron scattering, *Structure* **4**, 79–88.

Todd, M. J., Viitanen, P. V., and Lorimer, G. H. (1994) Dynamics of the chaperonin ATPase cycle: Implications for facilitated protein folding, *Science* **265**, 659–666.

Xu, Z., Horwich, A. L., and Sigler, P. B. (1997) The crystal structure of the asymmetric GroEL-GroES-$(ADP)_7$ chaperonin complex, *Nature* **388**, 741–750.

Zahn, R., Axmann, S. E., Rücknagel, K.-., Jaeger, E., Laminet, A. A., and Plückthun, A. (1994) Thermodynamic partitioning model for hydrophopic binding of polypeptides by GroEL, I. GroEL recognizes the signal sequences of β-lactamase precursor, *J. Mol. Biol.* **242**, 150–164.